Equivalent circuit modeling of dynamic hysteretic property of silicon steel under pulse width modulation excitation

AUTHOR(S):

Miyazaki, T.; Mifune, T.; Matsuo, T.; Shindo, Y.; Takahashi, Y.; Fujiwara, K.

CITATION:

Miyazaki, T. ...[et al]. Equivalent circuit modeling of dynamic hysteretic property of silicon steel under pulse width modulation excitation. Journal of Applied Physics 2015, 117(17): 17D110.

ISSUE DATE:

2015-02-09

URL:

http://hdl.handle.net/2433/197210

JOURNAL OF APPLIED PHYSICS **117**, 17D110 (2015)

Equivalent circuit modeling of dynamic hysteretic property of silicon steel under pulse width modulation excitation

T. Miyazaki,[1] T. Mifune,[1] T. Matsuo,[1,a)] Y. Shindo,[2] Y. Takahashi,[3] and K. Fujiwara[3]
[1]*Department of Electrical Engineering, Kyoto University, Kyoto 615-8510, Japan*
[2]*Kawasaki Heavy Industries, Ltd., Akashi 673-8666, Japan*
[3]*Department of Electrical Engineering, Doshisha University, Kyotanabe 610-0321, Japan*

(Presented 7 November 2014; received 22 September 2014; accepted 18 October 2014; published online 9 February 2015)

This paper describes the development of an efficient and accurate dynamic hysteresis model that combines the Cauer circuit representations with the play model. The physical meaning of the standard Cauer circuit is discussed and is used to derive a mathematical representation of hysteretic inductors. The iron-loss and hysteresis loops of silicon steel that were obtained using the proposed model agree with experimental data measured under sinusoidal and pulse width modulation excitations. © *2015 AIP Publishing LLC*. [http://dx.doi.org/10.1063/1.4907692]

I. INTRODUCTION

Pulse width modulation (PWM) excitation is commonly used for motor drive control. The high frequency components caused by PWM waveforms induce complex dynamic hysteretic magnetic fields in iron cores, where minor hysteresis loops and eddy-current fields with thin skin-depth are significant.

Several homogenization methods[1–3] have been proposed for the efficient analysis of laminated iron cores while avoiding finite-element division along the stacking directions of the steel sheets. However, accurate evaluation of the eddy-current field in a steel sheet with nonlinear magnetic properties is not easy without the use of sub-analysis methods,[1,3] including integral computation along the stacking direction.

A linear eddy-current theory is used to derive the standard and physical Cauer circuit representations[4,5] of the frequency-dependent properties of magnetic thin sheets, and these representations realize an accurate frequency response while using fewer elements than the series and parallel Foster circuit representations.[4] While the standard Cauer circuit is derived directly from the linear theory, the physical Cauer circuit also has been studied for the nonlinear magnetic properties modeling[2,5–7] because its physical meaning is clear. However, to describe nonlinear magnetic properties, the physical Cauer circuit requires more inductive elements than expected from the linear circuit, even after circuit optimization.[7]

From discussion of the physical meaning of the standard Cauer circuit, this study develops simple and efficient circuit representations to describe the dynamic hysteretic properties of silicon steel sheets. The representation accuracy of the proposed method is evaluated by comparison with experimental data measured under sinusoidal and PWM excitations.

II. CAUER REPRESENTATION

A. Linear theory

From linear eddy-current theory for magnetic thin sheets, the relationship between the average magnetic flux density B and the surface magnetic field H along the sheet is given as

$$B = \mu_c H, \tag{1}$$

$$\mu_c = \mu \frac{2}{kd} \tan \frac{kd}{2} = \mu \frac{2}{\mathrm{j}kd} \tanh \frac{\mathrm{j}kd}{2}, \tag{2}$$

where $k = \sqrt{-\mathrm{j}\omega\sigma\mu}$, ω is the angular frequency, μ is the permeability, σ is the conductivity, and d is the sheet thickness.

By expanding $\tan(kd/2)$ or $\tanh(\mathrm{j}kd/2)$, the relation given by (1) can be represented by an infinite resistor-inductor (RL) ladder circuit[4,5] as shown in Fig. 1, where $\mathrm{d}B/\mathrm{d}t$, H, μ, and $4/\sigma d^2$ are replaced by the terminal voltage v, the terminal current i, the inductance L, and the resistance R, respectively. This circuit is called the standard Cauer circuit. By truncating the standard Cauer circuit as shown in Fig. 2, it can be converted equivalently to another type of RL ladder circuit as shown in Fig. 3. This is called the physical Cauer circuit because the ratio of the inductances corresponds to the nonuniform physical division[3–7] of the half thickness of $d/2$.

B. Representation of hysteretic property

The static property of the standard Cauer circuit is given as $\Phi_1 = Li_1 = Li$. Accordingly, when the static magnetic property of a steel sheet has its nonlinearity represented by $H = h_{DC}(B)$, the inductor L is replaced by the relationship $i_1 = h_{DC}(\Phi_1)$. In the physical Cauer circuit, the k-th inductor L/α_k can be replaced by the relationship $i_k = h_{DC}(\alpha_k \Phi_k)$, because L/α_k corresponds to the magnetic flux passing through $1/\alpha_k$ of the sheet thickness. From a simple

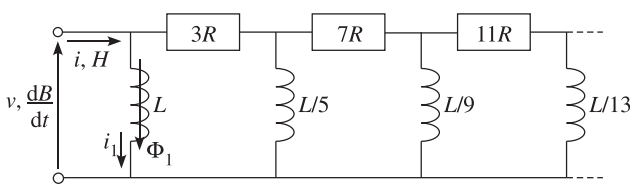

FIG. 1. Infinite RL ladder circuit.

a)Electronic mail: tmatsuo@kuee.kyoto-u.ac.jp.

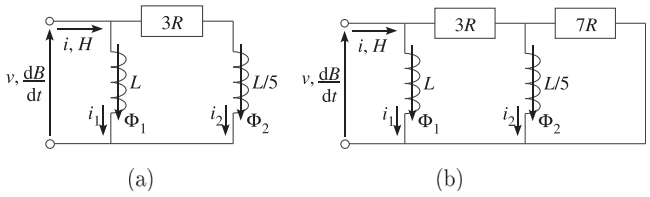

FIG. 2. Standard Cauer circuit: (a) inductive termination and (b) resistive termination.

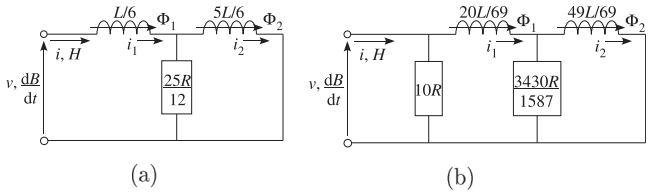

FIG. 3. Physical Cauer circuit: (a) corresponding to Fig. 2(a) and (b) corresponding to Fig. 2(b).

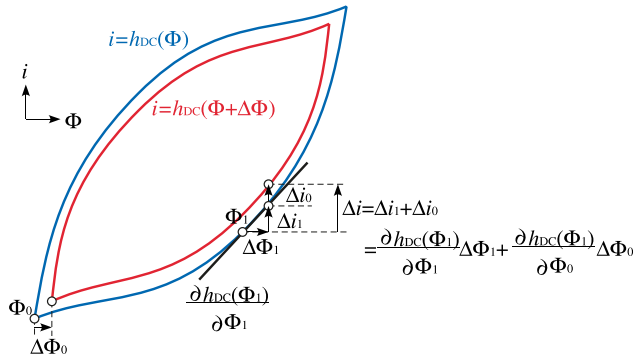

FIG. 4. Variation of i-Φ loop.

TABLE I. PWM waveforms list ($f_C = 2, 5, 10$ kHz).

	Modulation factor	B_{max}[T]	Full/half-bridge
No. 1	0.5	1.3	Full-bridge
No. 2			Half-bridge
No. 3		0.66	Full-bridge
No. 4			Half-bridge
No. 5	0.8	1.57	Full-bridge
No. 6			Half-bridge
No. 7		1.05	Full-bridge
No. 8			Half-bridge

interpretation based on similarity, the k-th inductor $L/(4k-3)$ in the standard Cauer circuit may be replaced by the relationship shown in (3), as follows:

$$i_k = h_{DC}((4k-3)\Phi_k). \tag{3}$$

On the other hand, the second inductor $L/5$ in the standard Cauer circuit can be physically interpreted as shown below. The standard Cauer circuit, when truncated only with L and $3R$, represents the classical eddy-current theory, and gives the relationship $H = h_{DC}(B) + (\sigma d^2/12)(dB/dt)$. Similar to classical eddy-current theory, the current i_2 is given approximately by $(d\Phi_1/dt)/(3R)$ for the low frequency field, which is regarded as the eddy-current induced by the flux change $d\Phi_1/dt$. On this basis, the magnetic flux Φ_2 that corresponds to $L/5$ is regarded as the secondary flux generated by the induced current i_2.

The explanation above is supported by the homogenization method in Ref. 3. It represents the magnetic flux density

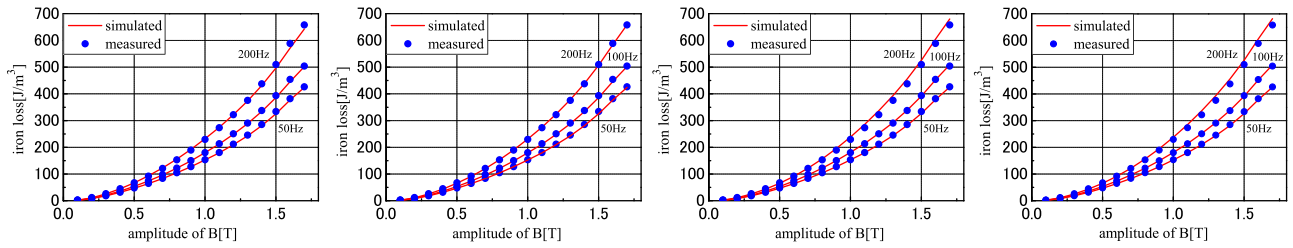

FIG. 5. Iron losses under sinusoidal excitation: (a) standard Cauer circuit with Eq. (3); (b) standard Cauer circuit with Eq. (10); (c) physical Cauer circuit; and (d) FEM.

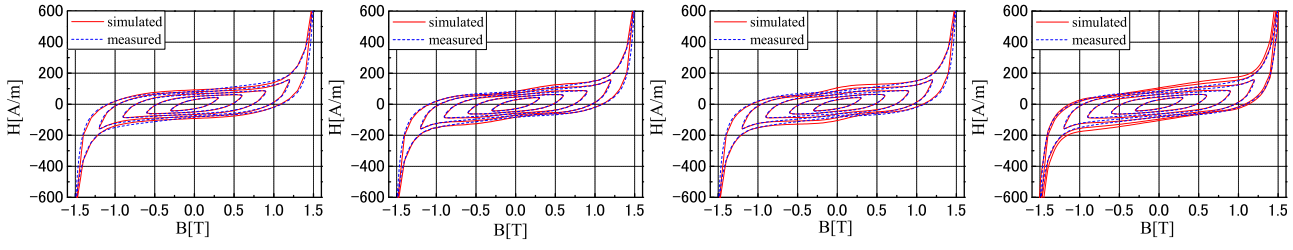

FIG. 6. BH loops under sinusoidal excitation: (a) standard Cauer circuit with Eq. (3); (b) standard Cauer circuit with Eq. (10); (c) physical Cauer circuit; and (d) FEM.

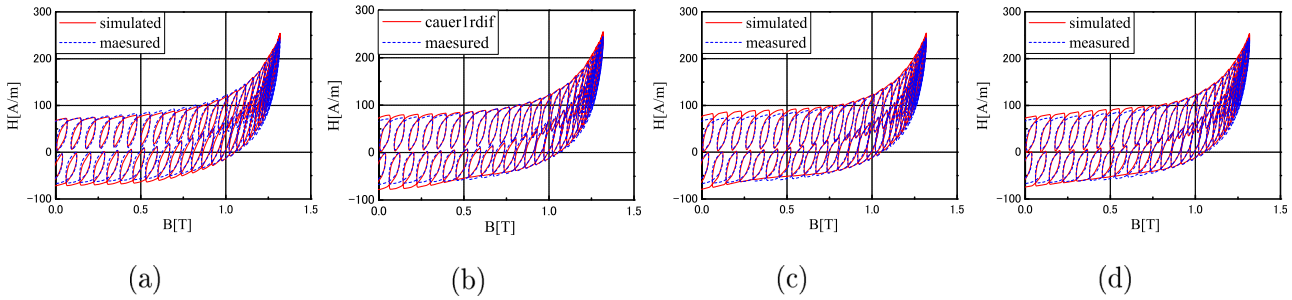

FIG. 7. BH loops under PWM excitation: (a) standard Cauer circuit with Eq. (3); (b) standard Cauer circuit with Eq. (10); (c) physical Cauer circuit; and (d) FEM.

TABLE II. Iron loss under PWM excitation.

	Carrier frequency 5 kHz								2 kHz	10 kHz
	Modulation factor 0.5				Modulation factor 0.8					
	1.30 T		0.66 T		1.57 T		1.05 T			
	Full	Half	Full	Half	Full	Half	Full	Half	Average error [%]	Average error [%]	Average error [%]
Measured [J/m^3]	161.8	82.9	592.5	280.0	222.6	170.5	559.2	401.6			
Standard Cauer w/Eq. (3) [J/m^3]	156.3	83.0	517.5	272.7	221.8	173.3	516.3	403.6	−3.50	−0.60	−2.86
Standard Cauer w/Eq. (10) [J/m^3]	163.3	83.9	584.4	289.0	229.8	175.3	550.6	412.3	1.98	0.65	1.15
Physical Cauer [J/m^3]	160.6	82.8	597.9	286.3	227.4	174.6	554.5	411.7	1.94	1.48	0.49
FEM [J/m^3]	160.6	83.1	590.6	286.3	227.2	174.8	550.5	412.0	1.63	1.06	0.67

distribution along the thickness direction $z\,(-d/2 \le z \le d/2)$ by a polynomial expansion as follows:

$$B(z,t) = \alpha_0(z)B_0(t) + \alpha_2(z)B_2(t) + \cdots, \tag{4}$$

$$\alpha_0(z) = 1, \quad \alpha_2(z) = -1/2 + 6(z/d)^2, \ldots. \tag{5}$$

In the linear case with permeability μ, B_0 and B_2 are governed by[3]

$$\begin{aligned} H(t) &= \frac{B_0(t)}{\mu} + \frac{\sigma d^2}{12}\frac{\mathrm{d}B_0}{\mathrm{d}t} - \frac{\sigma d^2}{60}\frac{\mathrm{d}B_2}{\mathrm{d}t} \\ 0 &= \frac{B_2(t)}{5\mu} - \frac{\sigma d^2}{60}\frac{\mathrm{d}B_0}{\mathrm{d}t} + \frac{\sigma d^2}{210}\frac{\mathrm{d}B_2}{\mathrm{d}t}, \end{aligned} \tag{6}$$

where all components of a higher order than B_2 are neglected. By replacing B_0, $B_2/5$, μ, and $4/(\sigma d^2)$ with Φ_1, Φ_2, L, and R, respectively, (6) can be rewritten as

$$\begin{aligned} H(t) &= \frac{\Phi_1(t)}{L} + \frac{1}{3R}\left(\frac{\mathrm{d}\Phi_1}{\mathrm{d}t} - \frac{\mathrm{d}\Phi_2}{\mathrm{d}t}\right) \\ 0 &= \frac{\Phi_2(t)}{L/5} - \frac{1}{3R}\left(\frac{\mathrm{d}\Phi_1}{\mathrm{d}t} - \frac{\mathrm{d}\Phi_2}{\mathrm{d}t}\right) + \frac{1}{7R}\frac{\mathrm{d}\Phi_2}{\mathrm{d}t}, \end{aligned} \tag{7}$$

which gives the circuit equation for the standard Cauer-circuit shown in Fig. 2(b). The uniformly distributed magnetic flux density B_0 induces an eddy-current that is distributed linearly along the z-direction, which yields the parabolically distributed B_2. This relationship corresponds to the relationship between Φ_1 and Φ_2.

Φ_2 can thus be regarded as a correction of the magnetic flux to Φ_1. When the correction is small and h_{DC} is not hysteretic, then the approximation below holds:

$$h_{\mathrm{DC}}(\Phi_1 + \Delta\Phi) \simeq h_{\mathrm{DC}}(\Phi_1) + \frac{\mathrm{d}h_{\mathrm{DC}}(\Phi_1)}{\mathrm{d}\Phi_1}\Delta\Phi. \tag{8}$$

However, when h_{DC} is a hysteretic function, the small variation $\Delta\Phi$ changes the hysteresis loop in the manner shown in Fig. 4. Both the variation $\Delta\Phi_1$ at $t = t_1$ and the variation $\Delta\Phi_0$ at the past time $t = t_0$ affect the hysteretic output of i at $t = t_1$ as follows:

$$\Delta i \simeq \frac{\partial h_{\mathrm{DC}}(\Phi_1)}{\partial \Phi_1}\Delta\Phi_1 + \frac{\partial h_{\mathrm{DC}}(\Phi_1)}{\partial \Phi_0}\Delta\Phi_0. \tag{9}$$

Rather than use $\partial h_{\mathrm{DC}}(\Phi_1)/\partial\Phi_0$, this study evaluates Δi directly using the finite difference $h_{\mathrm{DC}}(\Phi_1 + \Delta\Phi) - h_{\mathrm{DC}}(\Phi_1)$.

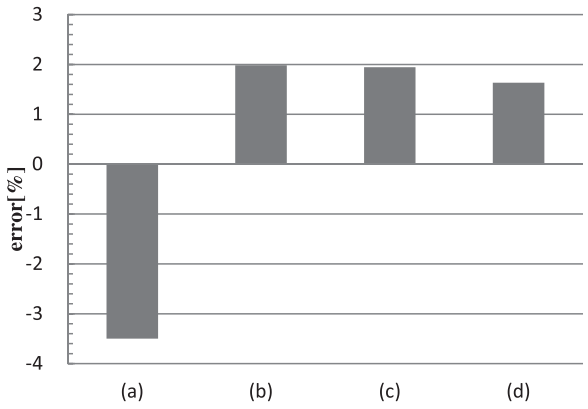

FIG. 8. Average evaluation error of iron losses given by four models: (a) standard Cauer circuit with Eq. (3); (b) standard Cauer circuit with Eq. (10); (c) physical Cauer circuit; and (d) FEM.

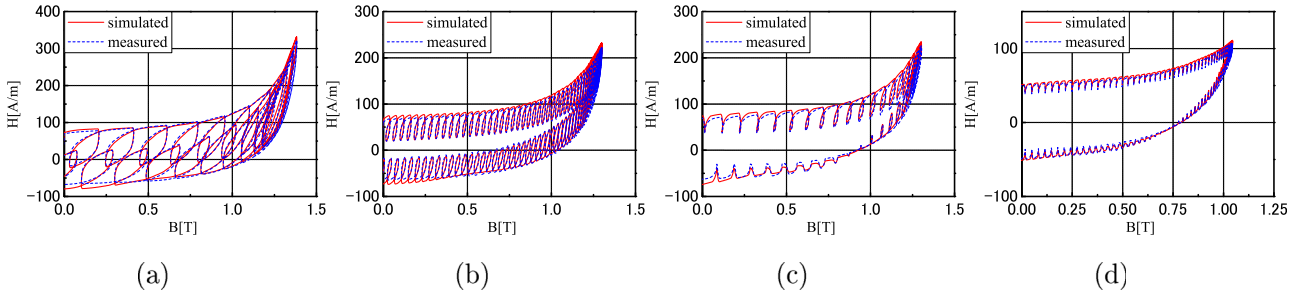

FIG. 9. BH loops obtained using standard Cauer circuit with Eq. (10): (a) waveform 1 with $f_C = 2$ kHz; (b) waveform 1 with $f_C = 10$ kHz; (c) waveform 2 with $f_C = 2$ kHz; and (d) waveform 8 with $f_C = 5$ kHz.

Consequently, the inductor $L/5$ in the standard Cauer circuit is replaced by the relationship

$$i_2 = 5[h_{DC}(\Phi_1 + \epsilon\Phi_2) - h_{DC}(\Phi_1)]/\epsilon\,, \tag{10}$$

where ϵ is a constant and h_{DC} is affected by the history of Φ_1 and $\Phi_1 + \epsilon\Phi_2$.

III. COMPUTATION RESULT

The magnetic properties of a non-oriented (NO) silicon steel sheet (JIS: 35A300) were measured under sinusoidal and PWM excitations. The thickness d of the steel sheet was 0.35 mm; the conductivity σ was 1.92×10^6 S/m. The dynamic hysteretic property was then simulated using the standard Cauer circuit shown in Fig. 2(b) with Eq. (3) or Eq. (10) and $\epsilon = 1$, and using the physical Cauer circuit in Fig. 3(b). The anomalous eddy-current loss is taken into account by multiplying the conductivity by the anomaly factor $k = 1.41$ to adjust the simulated eddy-current loss to match the measured loss at 50 Hz. In this study, the static property $h_{DC}(B)$ is represented by the play model[8] with input B. For comparison, a 1D finite-element eddy-current analysis was carried out by dividing the half thickness of $d/2$ into ten uniform elements.

A. Sinusoidal excitation

Figure 5 shows the computed iron loss per cycle under sinusoidal excitation at frequencies of 50, 100, and 200 Hz. The physical Cauer circuit and the finite element method (FEM) overestimate the iron loss at 200 Hz, whereas the standard Cauer circuit with Eq. (3) underestimates the loss. Figure 6 depicts the BH loops at 200 Hz, where the physical Cauer circuit yields a larger H than the measured data when B is small. The standard Cauer circuit with Eq. (10) obtains accurate iron losses and BH loops.

B. PWM excitation

Several PWM waveforms are listed in Table I and these waveforms are examined for excitation at the fundamental frequency of 50 Hz.

Figure 7 plots the BH loops for PWM waveform 1 with a carrier frequency (f_C) of 5 kHz. Use of the standard Cauer circuit with Eq. (3) results in smaller minor hysteresis loops, whereas use of the other methods obtains accurate representations. Table II compares the computed iron losses caused by the waveforms in Table I. Figure 8 shows the average evaluation error of the iron loss given by the four models with $f_C = 5$ kHz. As a result, the standard Cauer circuit with Eq. (10) achieves an accurate representation for both sinusoidal and PWM excitations. Figure 9 portrays the BH loops for PWM waveform 1 with $f_C = 2$ kHz and 10 kHz, PWM waveform 2 with $f_C = 2$ kHz, and waveform 5 with $f_C = 5$ kHz obtained using the standard Cauer circuit with Eq. (10), where the simulated loops all agree with the measured loops.

IV. CONCLUSION

Based on a discussion of the physical meaning of the standard Cauer circuit, a finite-difference representation of a hysteretic inductor is derived to describe the dynamic hysteretic properties of silicon steel sheets. The proposed standard Cauer circuit representation obtains accurate iron losses and BH loops under both sinusoidal and PWM excitations.

ACKNOWLEDGMENTS

This work was supported in part by a grant from the Kansai Research Foundation for Technology Promotion.

[1]O. Bottauscio, M. Chiampi, and D. Chiarabaglio, IEEE Trans. Magn. **36**, 561 (2000).
[2]J. H. Krah, A. Bergqvist, and G. Engdahl, IEEE Trans. Magn. **38**, 2385 (2002).
[3]J. Gyselinck and P. Dular, IEEE Trans. Magn. **40**, 856 (2004).
[4]Y. Shindo and O. Noro, IEEJ Trans. FM **134**, 173 (2014).
[5]E. J. Tarasiewicz, A. S. Morched, A. Narang, and E. P. Dick, IEEE Trans. Power Syst. **8**, 588 (1993).
[6]F. de León and A. Semlyen, IEEE Trans. Power Delivery **9**, 271 (1994).
[7]J. H. Krah, IEEE Trans. Magn. **41**, 1444 (2005).
[8]T. Matsuo and M. Shimasaki, IEEE Trans. Magn. **41**, 3112 (2005).